IMPROVED CARRIER TRANSPORT IN STRAINED Si/SiGe DEVICES

V. Palankovski, S. Dhar, H. Kosina, and S. Selberherr

Institute for Microelectronics, TU Vienna, Gusshausstrasse 27–29, A-1040 Vienna, Austria
Phone: +43-1-58801/36018, Fax: +43-1-58801/36099, Email: Dhar@iue.tuwien.ac.at

Abstract

Performance improvement in RFIC technology can be achieved by the introduction of novel materials and device structures. The SiGe/Si material system allows obtaining beneficial band structure and transport properties due to strain. This paper reviews recent theoretical and experimental achievements. Special focus is put on the description of the anisotropic majority/minority electron mobility in strained Si and SiGe layers as a function of doping and material composition. The Monte Carlo method is used for analyzing the transport properties of the strained Si/SiGe material system and for developing models for Technology Computer-Aided Design (TCAD) applications.

Introduction

In the last years, there has been enormous research in the area of materials compatible with Si technology and device structures for improving the speed of VLSI circuits. SiGe has emerged as a promising material because of its electrical and material properties. SiGe HBTs have found application in low-noise amplifiers and frequency dividers and have been combined with digital ICs (BiCMOS) for volume production. For the CMOS technology, although the SiGe channel has been used to enhance the performance of PMOS transistors, a desired improvement of the complimentary NMOS transistors is not achievable with SiGe. The replacement of the channel material by strained Si, which utilizes an underlying relaxed SiGe layer for its functioning, renders a solution to the problem since it leads to enhancement of both the electron and hole mobilities.

Strained Si/SiGe FETs exhibit superior performance for RF applications. Major developments have been reported by IBM [1, 2, 3, 4, 5, 6, 7, 8] and DaimlerChrysler (DC) [9, 10, 11, 12, 13, 14, 15, 16, 17, 18, 19, 20], both for p- and n-type devices. Fig. 1 summarizes reported values for the cut-off frequencies f_T and f_{max} in the last years.

In order to investigate and design strained SiGe (Si) device structures, it is necessary to model the carrier mobilities in these devices. This paper discusses the recent theoretical and experimental achievements reported for to describe the doping and material composition dependence for the strained Si material.

Physical Background

It is well known that due to lattice mismatch, a pseudomorphically grown SiGe (Si) layer on Si (relaxed SiGe) experiences a biaxial compressive (tensile)strain, provided that the layer thickness is below the critical thickness. This strain leads to a modification of both the conduction and valence bands. It lifts the degeneracy of the light and heavy hole bands and lowers the spin-orbit band resulting in reduction of inter-band scattering and improvement of hole mobility.

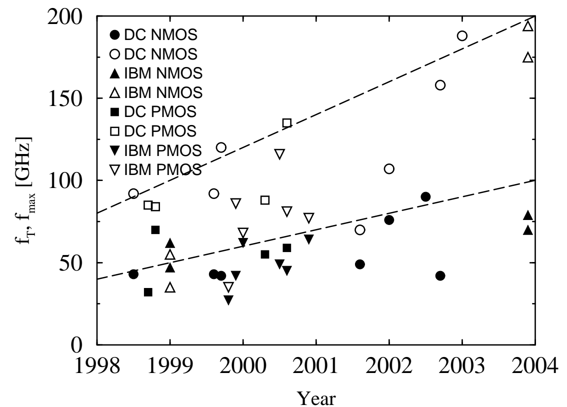

Figure 1: Cut-off frequencies f_T (filled symbols) and f_{max} (open symbols) of strained-Si FETs.

Since the conduction band structure in SiGe is silicon like for Ge< 0.85, compressively straining SiGe leads to splitting of the 6-fold degenerate Δ_6-valleys in Si into 2-fold degenerate Δ_2 valleys higher in energy and 4-fold degenerate Δ_4 valleys lower in energy. The higher in-plane effective electron mass of in Δ_4 valleys leads to a reduction of the electron mobility for strained SiGe. In the case of tensile strained Si, the direction of motion of the splitting is reversed with the Δ_4 valley moving lower in energy and Δ_4 higher. The lower in-plane effective mass of electrons in the Δ_2 valleys and the reduction of inter-valley phonon scattering lead to an enhanced electron mobility. Fig. 2 shows the band alignment of strained Si (SiGe) relative to relaxed SiGe and unstrained Si. The figure shows the strain-induced splitting of the conduction and valence bands, together with the band edge discontinuities, as a function of the ger-

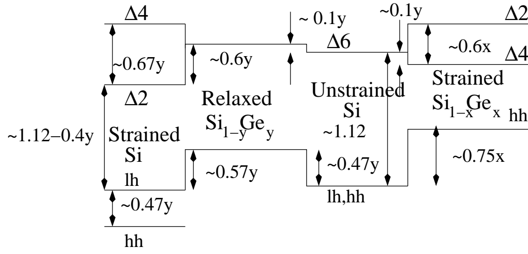

Figure 2: Bandgap alignment (in eV) of strained Si relative to relaxed $Si_{1-y}Ge_y$, strained $Si_{1-x}Ge_x$ and Si.

manium content y in the SiGe layer. In the calculations a linear dependence of the discontinuities on y has been assumed, which gives a good agreement with reported data [21].

Carrier Mobility Enhancement

Fig. 3a demonstrates the mobility enhancement ratio for electrons as a function of the germanium content y in the SiGe buffer layer. The mobility enhancement factor is defined as the ratio between the mobility in strained Si MOSFETs and the mobility in conventional Si MOSFETs. The figure compares experimental data from Stanford University [22, 23, 24], ERSO/ITRI [25], MIT [26, 27, 28, 29], IBM [30, 31, 32, 33], Hitachi [34], Toshiba [35, 36, 37, 38] TSMC [39], and Monte Carlo calculations from Vogelsang et al. [40], Rashed et al. [41], Takagi et al. [42], and our data. As can be seen in the figure the enhancement of the electron mobility increases gradually with the Ge content y for $y < 0.2$ and tends to saturate for higher values. It is remarkable that electron mobility enhancement of more than 50% is observed in a wide range of effective fields (up to 2 MV/cm) and doping concentrations (up to 6×10^{18} cm^{-3}) found in modern CMOS devices.

Fig. 3b shows the mobility enhancement ratio for holes as a function of the Ge content of the $Si_{1-y}Ge_y$ buffer layer. The figure compares experimental data from Stanford University [43], MIT [44], IBM [31, 32, 33], Hitachi [34], Toshiba [35, 38, 45, 46] to Monte Carlo calculations from Oberhuber et al. [47] and Bufler [48]. As can be seen the enhancement of the hole mobility increases gradually with the Ge content y for $y \leq 0.4$.

Modeling and Simulation

To enable predictive simulations using TCAD tools a reliable set of models for the Si/SiGe material system is required. Appropriate models for the band structure parameters and deformation potentials must be used. Pseudopotential calculations have been reported in [49, 50]. The transport properties of strained Si or SiGe layers have been theoretically investigated using Monte Carlo calculations [40, 51, 52, 53] or near equilibrium solutions to the Boltzmann equation [49]. A comprehensive set of strain-dependent models for parameters such as the low-field, high-field and the surface mobility, energy relaxation time and carrier life times for TCAD purposes is yet to be developed. Possible ap-

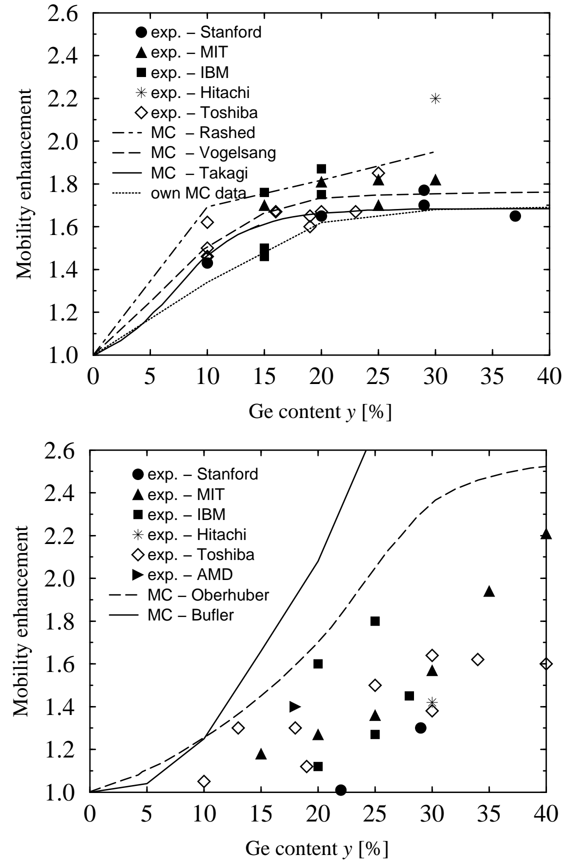

Figure 3: Mobility enhancement ratio for electrons (a) and holes (b) as a function of the Ge content y in the $Si_{1-y}Ge_y$ buffer layer.

proaches are to further use analytical models [54] or tabulated Monte Carlo data in a device simulator [55]. Strain effects on the device characteristics can be most comprehensively studied by Monte Carlo device simulation [56], however, at the expense of increased CPU-time requirements as compared to conventional TCAD simulation [57].

Modeling of the Electron Mobilities

The difference between majority and minority electron mobilities [58] is a well-known phenomenon caused by effects such as degeneracy and the different screening behavior of electrons and holes in the semiconductor. An analytical model which describes this effect based on Monte Carlo simulation data is given by (1)-(3) [59].

$$\mu^{\mathrm{LI}}_{\mathrm{n,maj}} = \frac{\mu^{\mathrm{L}}_{\mathrm{n}} - \mu^{\mathrm{mid}}_{\mathrm{maj}}}{1 + \left(\frac{N_{\mathrm{D}}}{C^{\mathrm{mid}}}\right)^{\alpha}} + \frac{\mu^{\mathrm{mid}}_{\mathrm{maj}} - \mu^{\mathrm{hi}}_{\mathrm{maj}}}{1 + \left(\frac{N_{\mathrm{D}}}{C^{\mathrm{hi}}_{\mathrm{maj}}}\right)^{\beta}} + \mu^{\mathrm{hi}}_{\mathrm{maj}} \tag{1}$$

$$\mu^{\mathrm{LI}}_{\mathrm{n,min}} = \frac{\mu^{\mathrm{L}}_{\mathrm{n}} - \mu^{\mathrm{mid}}_{\mathrm{min}}}{1 + \left(\frac{N_{\mathrm{A}}}{C^{\mathrm{mid}}}\right)^{\alpha}} + \frac{\mu^{\mathrm{mid}}_{\mathrm{min}} - \mu^{\mathrm{hi}}_{\mathrm{min}}}{1 + \left(\frac{N_{\mathrm{A}}}{C^{\mathrm{hi}}_{\mathrm{min}}}\right)^{\beta}} + \mu^{\mathrm{hi}}_{\mathrm{min}} \tag{2}$$

$$\mu^{\mathrm{LI}}_{\mathrm{n}} = 1/\left(1/\mu^{\mathrm{LI}}_{\mathrm{n,maj}} + 1/\mu^{\mathrm{LI}}_{\mathrm{n,min}} - 1/\mu^{\mathrm{L}}_{\mathrm{n}}\right) \tag{3}$$

$\mu^{\mathrm{L}}_{\mathrm{n}}$ is the mobility for undoped material, μ^{hi} is the mobility at highest doping. $\mu^{\mathrm{mid}}_{\mathrm{maj}}$, $\mu^{\mathrm{hi}}_{\mathrm{maj}}$, $\mu^{\mathrm{mid}}_{\mathrm{min}}$, $\mu^{\mathrm{hi}}_{\mathrm{min}}$, C^{mid}, $C^{\mathrm{hi}}_{\mathrm{maj}}$, $C^{\mathrm{hi}}_{\mathrm{min}}$, α, and β are used as fitting parameters. The

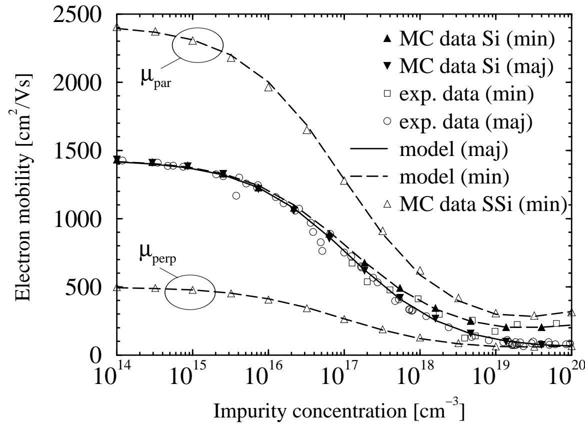

Figure 4: Majority and minority mobility in Si at 300 K: Comparison between Monte Carlo simulation data and experimental data.

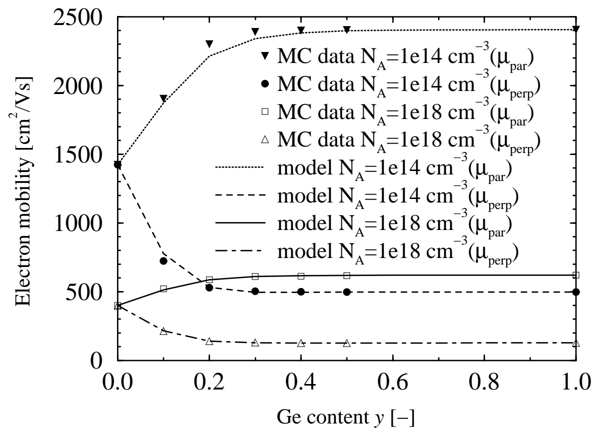

Figure 5: Minority electron mobility in strained Si as a function of the Ge content y in the $Si_{1-y}Ge_y$ buffer layer for different acceptor doping concentrations.

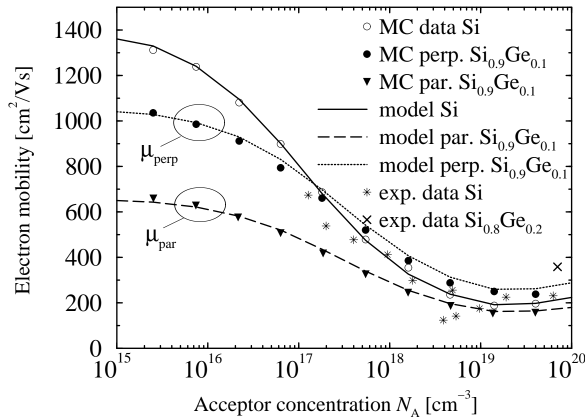

Figure 6: Minority electron mobility in $Si_{1-x}Ge_x$ as a function of N_A and x: Comparison with measurements and Monte Carlo simulation data for in-plane and perpendicular directions.

final low-field electron mobility μ^{LI}, which accounts for a combination of both acceptor and donor doping, is given by (3). Fig. 4 demonstrates a good match between the analytical model, our Monte Carlo simulation data, and measurements from [58, 60, 61, 62] for silicon at 300 K.

Table 1: Parameter values for the majority/minority electron mobility in strained SiGe and Si at 300 K

Parameter	Si	Ge(on Si)	SSi($\mu_{\parallel}$)	SSi($\mu_{\perp}$)
μ_n^{L} [cm^2/Vs]	1430	560	2420	502
μ_{maj}^{mid} [cm^2/Vs]	44	80	95	20
μ_{maj}^{hi} [cm^2/Vs]	57	59	123	25
μ_{min}^{mid} [cm^2/Vs]	141	124	232	49
μ_{min}^{hi} [cm^2/Vs]	218	158	315	62
α	0.65	0.65	0.65	0.65
β	2.0	2.0	2.0	2.0
C^{mid} [cm^{-3}]	1.12e17	4.0e17	8.6e16	8.3e16
C_{maj}^{hi} [cm^{-3}]	1.18e20	4.9e18	4.2e19	4.2e19
C_{min}^{hi} [cm^{-3}]	4.35e19	5.4e19	7.8e19	6.2e19

Monte Carlo simulation which accounts for alloy scattering and the splitting of the anisotropic conduction band valleys due to strain [63] in combination with an accurate ionized impurity scattering model [64], allowed us to obtain results for strained Si (SSi) for the complete range of donor and acceptor concentrations and Ge contents in the $Si_{1-y}Ge_y$ buffer layer. We use the same functional form (1)-(3) to fit the doping dependence of the in-plane and the perpendicular mobility component for $y = 0$ and $y = 1$ (Si and strained Si on Ge). Fig. 4 compares the analytical model with our Monte Carlo simulation data.

The material composition dependence is modeled by

$$\mu_n^{LI}(y) = \sum_{i=1}^{3} h^{(i)} \cdot p^{(i)} \cdot \mu_{n,uns}^{(i)}, \quad p^{(i)} = n_{str}^{(i)} / \sum_{i=1}^{3} n_{str}^{(i)} \tag{4}$$

$$h^{(i)} = \left(1 + r \cdot \left(\frac{3}{2} \cdot \left(1 - p^{(i)}\right)\right)^{\gamma}\right)^{-1}, \quad \gamma = 0.5 \tag{5}$$

$$r = (2\mu_{\parallel,y=1} + \mu_{\perp,y=1})/3\mu_{y=0}^{LI} - 1 \tag{6}$$

where $n_{str}^{(i)} = N_C^{(i)} \cdot \exp\left[\Delta E_C^{(i)}(y)/kT\right]$ denotes the strained electron population in the ith valley. $\mu_{n,uns}^{(i)}$ are the unstrained mobility tensors for [100], [010], and [001] X-valleys. (4) is a modification of (6.40) from [65]. An additional factor $h^{(i)}$ is incorporated to consider the effect of inter-valley scattering with γ as a fitting parameter.

Fig. 5 shows the in-plane (parallel) and the perpendicular minority electron mobility in strained Si as a function of y in the $Si_{1-y}Ge_y$ buffer at 300 K for different acceptor doping concentrations. Fig. 6 shows the minority electron mobility in strained $Si_{1-x}Ge_x$ as a function of acceptor concentration N_A in comparison with Monte Carlo simulation data both for in-plane and perpendicular directions.

It is remarkable that the electron mobility in perpendicular (vertical) direction is enhanced for typical base doping concentrations (above 10^{18} cm^{-3}) and typical Ge contents $x \leq 0.2$ in SiGe HBTs. The model parameters used for strained SiGe on Si and for strained Si on relaxed SiGe at 300 K are summarized in Table 1.

Device Simulation

Double-base SiGe HBTs with emitter areas of 12×0.4 μm^2 [59] have been analyzed by two-dimensional device simulation with MINIMOS-NT. Important physical effects, such as surface recombination, impact ionization generation, and self-heating, are properly modeled and accounted for in the simulation in order to get good agreement with measured DC characteristics using a concise set of models and parameters.

Fig. 7 illustrates the error in the estimation of the cut-off frequency f_T versus collector current I_C which can be introduced by ignoring the effect of the anisotropic electron mobility in the strained SiGe base. AC simulations [66] with anisotropic and isotropic mobility models are compared to measured data.

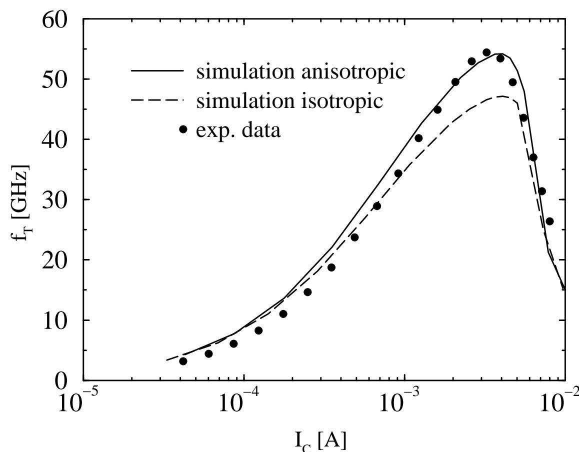

Figure 7: Cut-off frequency f_T versus collector current I_C at V_{CE} = 1 V for the SiGe HBT.

Conclusion

This work reviews carrier transport in strained Si MOSFETs and SiGe HBTs. Device performance is increased due to enhancement of both electron and hole mobilities compared to conventional Si devices. Mobility improvements by factors of more than two have been reported. TCAD simulation tools need correct models of the strained Si/SiGe material system, especially with respect to carrier transport. Experimental data remain a basic input for verification of analytical TCAD models. However, Monte Carlo simulation data with confirmed accuracy can deliver information which is still experimentally missing.

Acknowledgment

The authors acknowledge support from the Österreichische Forschungsgemeinschaft (ÖFG), Project MOEL-Plus 044, and the Semiconductor Research Corporation (SRC), Project 998.001.

References

[1] S. Koester *et al.*, Electron.Lett. **35**, 86 (1999).
[2] S. Koester *et al.*, Electron.Lett. **39**, 1684 (2003).
[3] W. Lu *et al.*, J.Vac.Sci.Technol.B **18**, 3488 (2000).
[4] S. Koester *et al.*, in *Proc. DRC* (2000), pp. 31–32.
[5] W. Lu *et al.*, IEEE Trans.Electron Devices **47**, 1645 (2000).
[6] S. Koester *et al.*, in *Proc. EDMO* (1999), pp. 27–32.
[7] W. Lu *et al.*, in *IEDM Tech.Dig.* (1999), pp. 577–580.
[8] W. Lu *et al.*, IEEE Electron Device Lett. **20**, 514 (1999).
[9] M. Enciso *et al.*, Electron.Lett. **37**, 1089 (2001).
[10] N. Zerounian *et al.*, in *Proc. ESSDERC* (1999), pp. 296–269.
[11] U. Konig *et al.*, Solid-State Electron. **43**, 1383 (1999).
[12] M. Gluck *et al.*, Physica E **2**, 763 (1998).
[13] F. Aniel *et al.*, in *Proc. ESSDERC* (2002), pp. 167–170.
[14] M. Enciso *et al.*, Electron.Lett. **39**, 149 (2003).
[15] M. Zeuner *et al.*, in *Proc. DRC* (2002), pp. 53–54.
[16] F. Aniel *et al.*, in *Proc. DRC* (2001), pp. 482–485.
[17] G. Hock *et al.*, Electron.Lett. **36**, 1428 (2000).
[18] G. Hock *et al.*, in *Digest Topical Meetings on Si MICs in RF Systems* (2000), pp. 156–158.
[19] G. Hock *et al.*, Electron.Lett. **34**, 1888 (1998).
[20] U. Konig *et al.*, J.Vac.Sci.Technol.B **16**, 2609 (1998).
[21] C. Maiti *et al.*, *Strained silicon heterostructures: materials and devices* (IEE, 2001).
[22] J. Welser *et al.*, in *IEDM Tech.Dig.* (1992), pp. 1000–1002.
[23] J. Welser *et al.*, in *IEDM Tech.Dig.* (1994), pp. 373–376.
[24] J. Welser *et al.*, IEEE Electron Device Lett. **15**, 100 (1994).
[25] M. Lee *et al.*, in *IEDM Tech.Dig.* (2003), pp. 69–72.
[26] M.-T. Currie *et al.*, J.Vac.Sci.Technol.B **19**, 2268 (2001).
[27] Z.-Y. Cheng *et al.*, IEEE Electron Device Lett. **22**, 321 (2001).
[28] H.-M. Nayfeh *et al.*, in *IEDM Tech.Dig.* (2003), pp. 475–478.
[29] I. Lauer *et al.*, IEEE Electron Device Lett. **25**, 83 (2004).
[30] K. Rim *et al.*, in *IEDM Tech.Dig.* (1998), pp. 707–710.
[31] K. Rim *et al.*, in *VLSI Symp. Tech.Dig.* (2001), pp. 59–60.
[32] L.-J. Huang *et al.*, in *VLSI Symp. Tech.Dig.* (2001), pp. 57–58.
[33] K. Rim *et al.*, in *VLSI Symp. Tech.Dig.* (2002), pp. 98–99.
[34] N. Sugii *et al.*, in *IEDM Tech.Dig.* (2001), pp. 737–740.
[35] T. Mizuno *et al.*, IEEE Electron Device Lett. **21**, 230 (2000).
[36] T. Tezuka *et al.*, in *VLSI Symp. Tech.Dig.* (2002), pp. 96–97.
[37] T. Mizuno *et al.*, IEEE Trans.Electron Devices **49**, 7 (2002).
[38] S. Takagi, in *Proc. DRC* (2002), pp. 37–40.
[39] H.-H. Wang *et al.*, in *IEDM Tech.Dig.* (2003), pp. 61–64.
[40] T. Vogelsang and K. Hofmann, Appl.Phys.Lett. **63**, 186 (1993).
[41] M. Rashed *et al.*, in *IEDM Tech.Dig.* (1995), pp. 765–768.
[42] S. Takagi *et al.*, J.Appl.Phys. **80**, 1567 (1996).
[43] K. Rim *et al.*, in *IEDM Tech.Dig.* (1995), pp. 517–520.
[44] C.-W. Leitz *et al.*, J.Appl.Phys. **92**, 3745 (2002).
[45] T. Mizuno *et al.*, in *VLSI Symp. Tech.Dig.* (2002), pp. 106–107.
[46] T. Mizuno *et al.*, in *VLSI Symp. Tech.Dig.* (2000), pp. 210–211.
[47] R. Oberhuber *et al.*, Phys.Rev.B **58**, 9941 (1998).
[48] F. Bufler, *Full-Band Monte Carlo Simulation of Electrons and Holes in Strained Si and SiGe* (Herbert Utz Verlag, 1998).
[49] M. Fischetti and S. Laux, J.Appl.Phys. **80**, 2234 (1996).
[50] M. Rieger and P. Vogl, Phys.Rev.B **48**, 14276 (1993).
[51] L. Kay and T.-W. Tang, J.Appl.Phys. **70**, 1483 (1991).
[52] F. Bufler *et al.*, Appl.Phys.Lett. **70**, 2144 (1997).
[53] B. Fischer, *A full-band Monte Carlo charge transport model for nanoscale silicon devices including strain* (Shaker Verlag, 2000).
[54] J. Roldan *et al.*, IEEE Trans.Electron Devices **50**, 1408 (2003).
[55] F. Gamiz *et al.*, IEEE Trans.Electron Devices **48**, 1878 (2001).
[56] F. Bufler and W. Fichtner, IEEE Trans.Electron Devices **50**, 2461 (2003).
[57] Binder *et al.*, *MINIMOS-NT Device and Circuit Simulator, User's Guide, Release 2.0*, Institut für Mikroelektronik, TU Wien, 2002, http://www.iue.tuwien.ac.at/mmnt.
[58] G. Masetti *et al.*, IEEE Trans.Electron Devices **ED-30**, 764 (1983).
[59] V. Palankovski and R. Quay, *Analysis and Simulation of Heterostructure Devices* (Springer, Wien, New York, 2004).
[60] I. Leu and A. Neugroschel, IEEE Trans.Electron Devices **40**, 1872 (1993).
[61] S. Swirhun *et al.*, in *IEDM Tech.Dig.* (1996), pp. 24–27.
[62] K. Wolfstirn, J.Phys.Chem.Solids **16**, 279 (1960).
[63] S. Smirnov *et al.*, in *Proc. SISPAD* (2002), pp. 29–32.
[64] H. Kosina and G. Kaiblinger-Grujin, Solid-State Electron. **42**, 331 (1998).
[65] A. Nathan and H. Baltes, *Microtransducer CAD* (Springer Verlag, Wien, New York, 1999).
[66] S. Wagner *et al.*, Applied Surface Science **224**, 365 (2004).